THE MOBILITY OF EDGE DISLOCATIONS IN THE BASAL SLIP SYSTEM OF ZINC

Thesis by

David Peter Pope

In Partial Fulfillment of the Requirements

For the Degree of

Doctor of Philosophy

California Institute of Technology

Pasadena, California

1967

(Submitted January 6, 1967)

ACKNOWLEDGMENTS

The author wishes to thank Professor T. Vreeland, Jr. for his continued interest and encouragement during the course of this work. Appreciation is extended to Professor D. S. Wood for his many helpful suggestions and comments. Thanks are extended to Professor D. S. Clark, who made many helpful suggestions concerning this manuscript. Thanks are also expressed to Mr. G. R. May for his assistance in specimen preparation.

The author is indebted to the R. C. Baker Foundation for fellowship grants. The research was performed under a contract with the United States Atomic Energy Commission.

The author wishes to extend special thanks to his wife, Myrna, whose patience and understanding made this work possible.

ABSTRACT

This thesis presents the results of measurements of the velocities of edge dislocations in the basal slip system of zinc as a function of applied shear stress. All tests were conducted at room temperature on 99.999 per cent purity zinc monocrystals. Dislocations were revealed by means of the Berg-Barrett x-ray technique. Stress pulses of microsecond duration were applied to the test specimens by means of a torsion testing machine. Applied resolved shear stresses ranged from 0 to 17.2×10^6 dynes/cm^2 and measured dislocation velocities ranged from 40 to 700 cm/sec.

The results of this study indicate that the velocity of edge dislocations in the basal slip system of zinc is linearly proportional to the applied resolved shear stress. These results are analyzed in terms of the phonon drag theory. Agreement between this theory and the results reported in this thesis is quite good. Further work is suggested that will provide a more definitive test of the phonon drag theory for limiting dislocation motion in metallic crystals.

TABLE OF CONTENTS

LIST OF FIGURES

I. INTRODUCTION

Plastic flow of crystalline solids is a result of the motion and multiplication of the dislocations contained within the solid. Therefore, a knowledge of how dislocations move and multiply under the influence of an applied resolved shear stress is necessary for a fundamental understanding of crystal plasticity. This thesis presents data obtained relating the velocity of individual basal dislocations in zinc to the applied shear stress.

The plastic strain rate of a crystalline solid is related to the average dislocation behavior through the expression:

$$\dot{\gamma} = \rho_m b \bar{v} \qquad [1]$$

where $\dot{\gamma}$ is the plastic shear strain rate, ρ_m is the total length of moving dislocation line per unit volume, b is the slip or Burgers vector of the dislocations, and $\bar{v}$ is the average velocity of the dislocations. Equation 1, together with experimentally determined values of ρ_m and $\bar{v}$, has led to some impressively successful applications of dislocation theory to a wide range of plastic flow phenomena. For example, W. G. Johnston who, together with J. J. Gilman made the first measurements of velocities of individual dislocations (1), has used these data to predict stress-strain curves exhibiting yield points (2). Li has used dislocation mobility and density data to describe transient creep (3). Perhaps most impressive of all, Taylor has used mobility data to explain some aspects of high velocity impact experiments (4). None of these phenomena could be explained by classical plasticity theory. It is now more than a statement of faith to say that

dislocation theory has real promise for playing a predictive rather than an explanatory role in future materials behavior.

There has been considerable dislocation mobility data gathered on various materials in recent years. The materials on which these measurements have been made are lithium fluoride (1), silicon-iron (5), sodium chloride (6), tungsten (7), various semiconductor crystals (8, 9), zinc (10), and copper (11). The data on zinc (10) were measured over quite a restricted stress and velocity range due to testing equipment limitations. It should be noted that all the crystals mentioned above except zinc and copper have either covalent or ionic bonding or have a BCC crystal structure. Dislocations in these materials move at velocities far less than one cm/sec at the macroscopic yield point. However, in copper and zinc, an FCC metal and a HCP metal respectively, the dislocations move at velocities well over one cm/sec at the yield point. The paucity of mobility data on FCC and HCP metals, materials in which the dislocations move rapidly at low stresses, is not due to a lack of interest in these materials but rather due to the lack of suitable experimental techniques for handling and testing these very fragile crystals. It is the scarcity of mobility data on these materials that prompted the work reported here.

The experimental methods used in determining dislocation velocities can be conveniently divided into two classes, the direct and indirect methods. In the direct experiments, individual dislocations or dislocation groups are observed continuously during loading or before and after loading. The most important aspect of the direct

experiments is that it is the dislocations themselves that are observed in these experiments. However, in the indirect experiments, dislocation velocities are deduced from the measurement of macroscopic parameters, such as stress, strain, strain rate, and internal friction. Dislocation velocities are deduced by assuming an a priori dependence of dislocation velocity on the measured parameters. These techniques will be further discussed later in this thesis. The direct experiments are not dependent upon assumptions relating macroscopic behavior to dislocation velocities for their interpretation, although they do require the use of certain other assumptions such as the assumption that the dislocation velocities are in phase with the stress; i.e., the time for a dislocation to reach its terminal velocity at a given stress is small compared to the loading time.

Straining a foil in the stage of an electron microscope is perhaps the most obvious choice for a direct experiment because individual dislocations can be observed continuously as they move. Unfortunately, in this method it is almost impossible to measure the stress in the foil and there is no guarantee that the dislocation behavior in foils a few hundred Å thick approximates the behavior in bulk crystals. Hence, quantitative mobility data have not been gathered by means of this technique. The etch pit technique has been the most widely used method of dislocation observation for direct measurement of dislocation velocities. With this technique the sites where dislocations initially intersect the specimen surfaces are revealed by a suitable chemical etchant. A load pulse of known magnitude and duration is applied to the specimen and the specimen is then re-

etched to determine the final dislocation positions. Dislocation velocities are determined by dividing the dislocation displacements by the pulse duration. This is the technique used by Johnston and Gilman in their pioneering experiments on lithium fluoride (1). A third technique, the one used in the work reported here, reveals individual dislocation lines before and after loading by means of an x-ray diffraction technique. A dislocation must lie within a few microns of the specimen surface to be revealed by this technique. A similar technique has been used in one other investigation (12).

Indirect experiments are appealing mainly because they are generally less tedious toperform than direct experiments. In one such experiment (13), the strain rate in a specimen subjected to uniaxial compression is changed discontinuously with time and the change in stress is observed. The changes in strain rate and stress are then related to the dislocation velocities through equation 1 assuming that ρ_m is constant. Unfortunately, this assumption has been shown to be incorrect in several materials in which both the strain rate experiment and direct experiments have been performed. In another indirect experimental approach the acoustic damping of high frequency, small amplitude strain waves in a crystal is measured as a function of frequency. To interpret the data, it is assumed that the dislocation velocity $\bar{v}$ is related to the applied shear stress τ by the relation

$$\bar{v} = A\tau \qquad [2]$$

where A is a constant. However, most materials on which direct experiments have been performed obey the empirical relation

$$\bar{v} = B\tau^m \qquad [3]$$

where m is a constant between about 2 and 35. The only materials in which the dislocations obey equation 2 are copper (7) and zinc, as determined in the work reported here. The acoustical damping measurements yield the ratio A/ρ_m. Hence, the accuracy with which A is known is no better than the accuracy with which ρ_m is known.

The studies made by Adams (10) exhibited two important facts about mobility measurements of basal dislocations in zinc; basal dislocations move rapidly at low stresses, and the indirect strain rate measurements yield results very different from direct measurements. Thus, it was decided to embark on an experimental program to make direct measurements of basal dislocation velocities as a function of applied shear stress in high purity (99.999 per cent), low dislocation density zinc single crystals. In this first series of tests, the velocities are measured as a function of applied shear stress only.

To measure large dislocation velocities, it is necessary to devise a loading system that will apply stresses for durations short enough that the dislocations being observed do not move out of the specimen or become lost in the background dislocation density. From Adams' work it was clear that loading times of microsecond duration would be necessary. Single crystals were used so that the manifold complications due to changes in crystal orientation across grain boundaries could be avoided. Zinc of 99.999 per cent purity was used so that the mobility data obtained would not be unduly affected by impurities.

A long series of preliminary tests showed that the double etch technique, the technique successfully used in copper (11), was not

suitable for these experiments on zinc. First, the basal dislocation density could not be reduced to a level where it was possible to follow the displacement of an individual dislocation and second, sources of large numbers of mobile dislocations could not be produced at selected, isolated sites in zinc. If these sources could be produced, perhaps the motions of large groups of dislocations could be observed even with a high background density.

It was found that by using the Berg-Barrett x-ray diffraction method for dislocation observations, both of the above mentioned problems were avoided. Furthermore, the Berg-Barrett method yields an image of the dislocation line as opposed to the etch technique which shows only the intersections of dislocations with free surfaces. Also, the x-ray technique allows the determination of the Burgers vector of individual dislocations. Thus, the Berg-Barrett technique yields considerably more information about the dislocations being observed than does the etch technique.

All tests were conducted at room temperature on high purity, annealed zinc monocrystals machined into right circular cylinders. The longitudinal axes of the cylinders were parallel to the crystallographic c axis and the ends were parallel to the basal plane. Edge dislocations were produced on one end of each specimen by scratching the surface with an Al_2O_3 whisker loaded with 50 mg. The scratched surface of the specimen was glued to a loading fixture and a torsion pulse of about 50 to 100 microseconds duration was applied to the specimen. The final dislocation configuration around the scratches was observed by means of the Berg-Barrett x-ray technique.

Experimental techniques, data reduction methods, and experimental results are reported in Parts II through IV of this thesis. Part V discusses these data in the light of currently existing theories of dislocation motion and compares the mobility of dislocations in zinc with the mobility of dislocations in other materials. Part VI reports the conclusions which can be drawn from the data and discusses further work which should be done in this area.

III. TEST SPECIMEN PREPARATION

The specimen composition, shape, and orientation were selected on the basis of a wide variety of considerations. The important considerations used in making these selections are listed below.

1. Zinc of high purity is required so that the effect of unknown impurities on dislocation velocities can be minimized.

2. Monocrystalline samples are desired since changes in crystallographic orientation across grain boundaries introduce great complications in the stress state. Furthermore, single crystals are preferred when the Berg-Barrett x-ray technique is used, since this technique utilizes the Bragg reflection from a single set of crystallographic planes. An entire specimen surface of a monocrystalline sample can be imaged rather than a few isolated grains.

3. When a stress pulse is applied to a specimen, it is desirable that the plastic strains in the specimen be small compared to the elastic strains. If plastic strains are larger, the stress pulse shape and the spatial stress distribution in the specimen become very complicated. Therefore, it is desirable to minimize the bulk basal dislocation content in the specimens.

4. The torsion loading system developed for this work accommodates specimens in the shape of right circular cylinders. The longitudinal axis of a specimen must be the crystallographic c axis so that the applied torque results in a simple stress state in the specimen. With this orientation, a torque applied about the longitudinal axis produces a shear stress τ on the basal plane

$$\tau = Tr/J \qquad [4]$$

where T is the torque, r is the distance from the specimen axis, and J is the polar moment of the cross section.

5. The angle between the basal slip plane and the observation surface must be small compared to 0.15° in order to use the Berg-Barrett x-ray technique. If the free surface were inclined at a greater angle to the slip plane, dislocations would glide out of the specimen or glide beneath the 5μ x-ray penetration depth when undergoing displacements of the desired magnitude. Undulations of the observation surface must be small compared to 5μ for the same reason. An end surface of the cylindrical specimens was prepared to meet these requirements.

6. The oxide coating on the observation surface must be thin compared to 5μ to allow sharp x-ray photographs to be taken through this layer. Contamination of this surface must be avoided both to prevent excessive oxide formation and to avoid the introduction of impurities into the 5μ layer in which dislocations can be observed.

7. The subgrains must be larger than the desired dislocation displacements (0.040 cm). The angular misorientation across the subgrain boundaries should be much less than 1° to allow a Bragg reflection from a large portion of the specimen surface.

8. The dislocation density within the subgrains must be low enough so that a given dislocation can be located after undergoing a displacement of about 0.040 cm.

Single crystals were grown from 99.999 per cent pure zinc obtained from Eagle-Picher Company, Miami, Oklahoma. The crystals were grown in graphite-coated pyrex molds 3.5 cm in di-

ameter and 25 cm long. The growth technique has been described by Stofel (14). After the bulk crystal was removed from the pyrex mold, the orientation of the basal plane was determined by cleaving a piece of the crystal in liquid nitrogen. Great care was taken to cool and heat the material no faster than $3^{\circ}C$/min to avoid plastic strains due to non-uniform thermal expansion. The bulk crystal was then acid cut into rough cylinders with (0001) axes and having at least one cleaved basal plane end. The plastic strains caused by this cutting operation were minimized by sawing the specimens with a stainless steel wire wetted in 50 per cent HNO_3. The cleaved basal plane of the rough cylinder was then glued to a block of monel alloy R405 using Duco cement. Monel R405 alloy was used because its coefficient of thermal expansion closely matches that of zinc in the basal plane. The specimen was then placed in an acid lathe similar to that used in reference 14 and turned to 1.10 cm diameter. In the acid lathe the specimen is rotated about its longitudinal axis while being held lightly against the curved surface of a cloth coated, 50 per cent HNO_3 wetted, rotating wheel. The specimen holding assembly is supported by two double pendulums which employ thin flexures as hinges. The flexures limit the force which holds the specimen against the wheel. Observation surfaces of test specimens were prepared either by cleaving or acid lapping. The acid lapped surfaces were prepared on a machine which is similar to the acid lathe. In this machine, the specimen is rotated about its longitudinal axis while one end is held very lightly against the flat surface of a rotating teflon wheel wetted with 50 per cent HNO_3. Again, the specimen

holding assembly is supported by two pendulums using flexures for hinges. The specimen was then polished as described in reference 15. Finished specimens were from 0.97 to 1.3 cm long.

All specimen surfaces had to be very clean to prevent contamination of the testing surface during annealing. The specimens were annealed in pure hydrogen at 370°C for $\frac{1}{2}$ to 3 hours. The hydrogen was purified by diffusion through a commercially available palladium purification unit. Specimens with an acid lapped observation surface were ready for testing after this anneal. However, two separate annealing operations were required during the production of a specimen with a cleaved test surface, the first anneal making it easier to subsequently produce a smooth, step-free cleavage surface. Berg-Barrett photographs of annealed specimens showed only a few isolated basal dislocations inside the subgrains. The low dislocation density is typical of the material very near the observation surface and is not typical of the bulk material. This low dislocation density is due to the ease with which dislocations near the surface can climb and/or cross glide out of the specimen during the anneal.

III. EXPERIMENTAL TECHNIQUES

Method for Producing Dislocations to Be Studied

Edge dislocations were produced by scratching the basal plane observation surface of the test specimens by means of the apparatus shown in Figure 1. Three scratches, each made on a diameter along the $<10\bar{1}0>$ directions, were made by an Al_2O_3 whisker fastened to an arm supported by a calibrated torsion wire. The force on the whisker was 50 mg. The scratches were made in segments approximately 0.050 cm long with 0.008 cm gaps between each segment. Subsequent Berg-Barrett photographs showed the dislocations produced to be edge oriented and lying in the basal plane with $<11\bar{2}0>$ type Burgers vectors.

X-Ray Technique for Observing Dislocations

Dislocations in the basal plane were observed by means of the Berg-Barrett x-ray technique as used by Armstrong and Schultz (16) for photographing zinc. Since the theory of this technique is adequately treated elsewhere (17), only a short description will be given here. As shown in Figure 2, x-rays from the source A are collimated by the slit B , diffracted from the specimen C and recorded on the photographic plate D. The photographic plate is placed nearly parallel to the incident x-ray beam yielding an unmagnified and slightly distorted image of the specimen. Figure 3 shows a photograph of the apparatus used. The width of the image of the dislocation line on the photographic plate is approximately given by (x-ray focal spot size) $\times$ (specimen to film distance)/(x-ray source to specimen

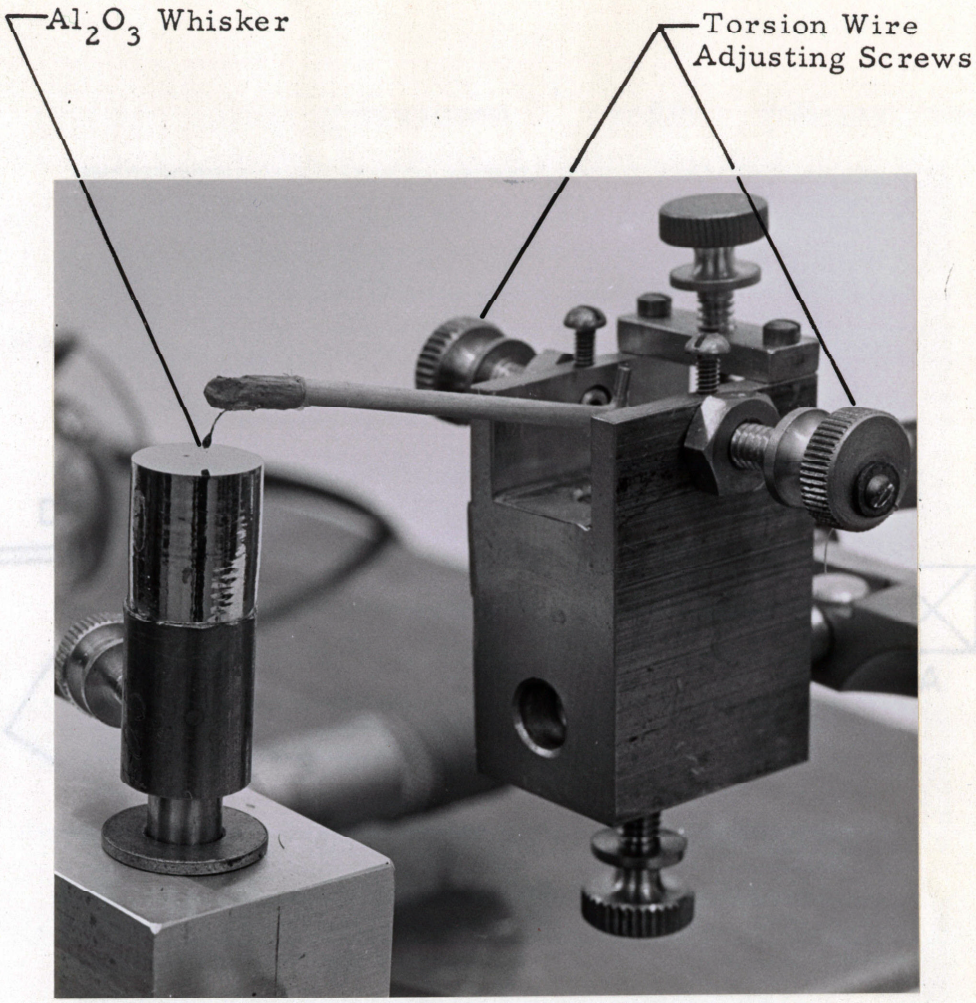

Figure 1. Scratching Apparatus and Test Specimen.

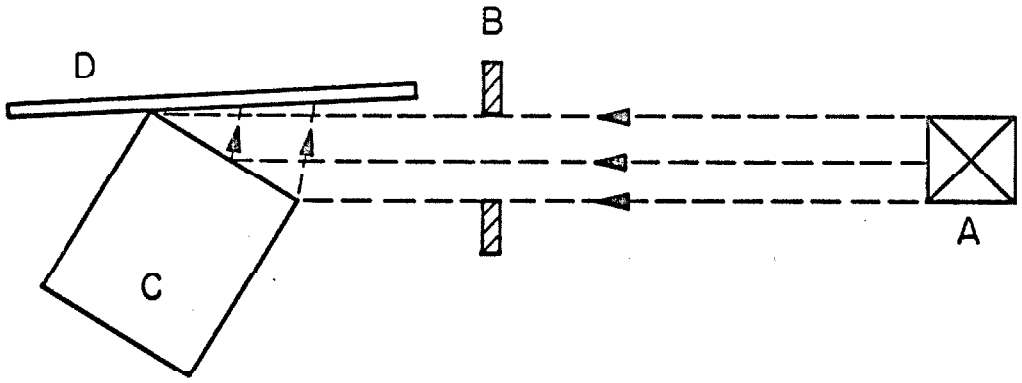

Figure 2. Schematic Diagram of Berg-Barrett Apparatus.

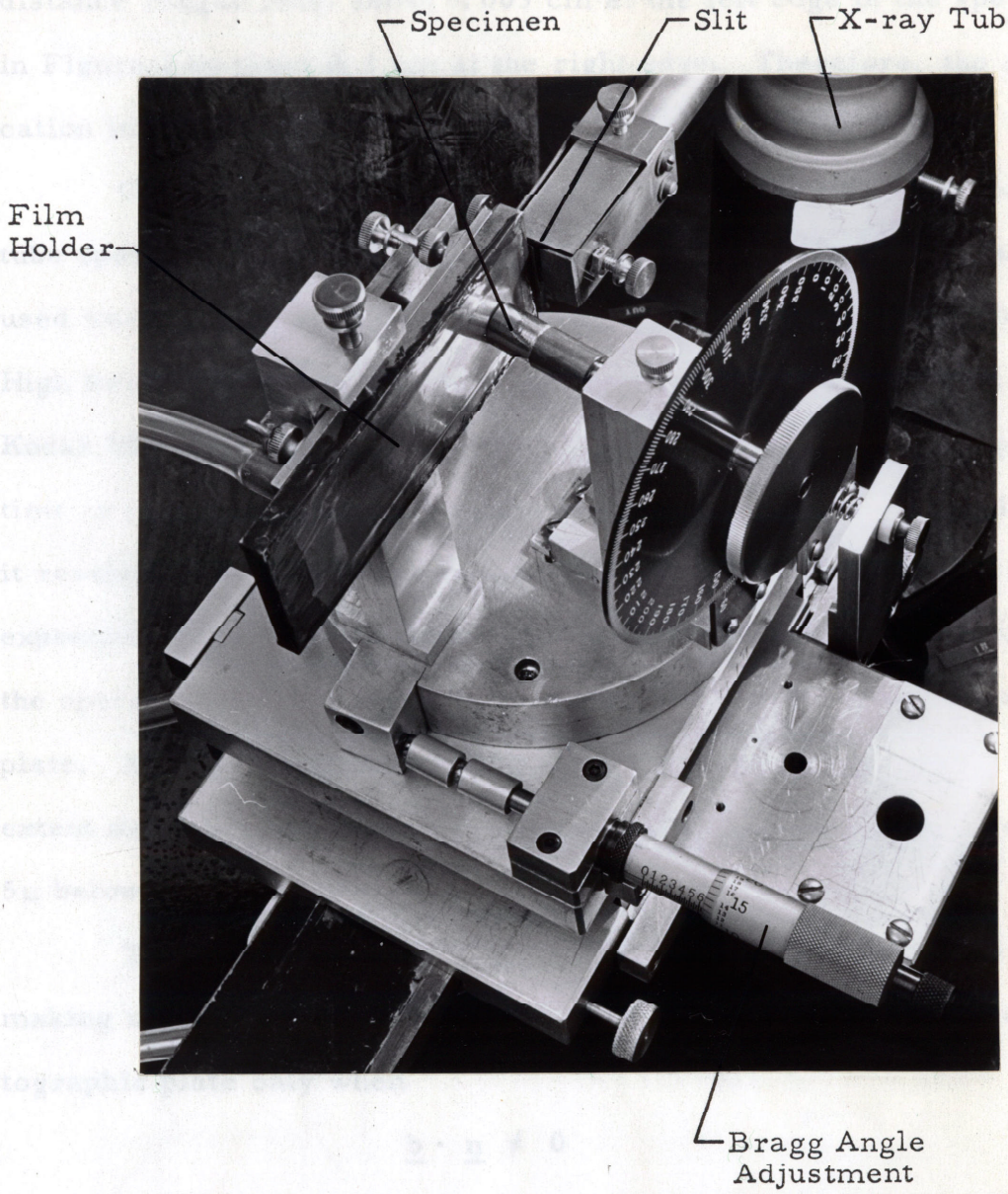

Figure 3. Photograph of Berg-Barrett X-Ray Apparatus.

distance). In this work, the focal spot size was 1 mm, the x-ray source to specimen distance was 15 cm, and the specimen to film distance ranged from about 0.003 cm at the left edge of the specimen in Figure 2 to about 0.1 cm at the right edge. Therefore, the dislocation image widths varied from 0.2μ to 7μ.

Characteristic Co radiation from a Machlett A-2 diffraction tube operating at 39 KV and 9 ma was used. The reflecting planes used were the $\{10\bar{1}3\}$ planes. The images were recorded on Kodak High Resolution plates exposed for 6 to 8 hours, and developed in Kodak HRP developer for 5 to 7 minutes at 23°C. This development time is considerably longer than the time recommended by Kodak, but it resulted in no great loss in image quality and a great saving in exposure time. An iron filter 0.0025 cm thick was placed between the specimen and film to prevent any fluorescence from reaching the plate. X-rays of the wave length used are absorbed by zinc to the extent that only those dislocations are imaged which lie within a layer 5μ below the observation surface.

The Burgers vector of a dislocation may be determined by making use of the fact that a dislocation produces an image on a photographic plate only when

$$\underline{b} \cdot \underline{n} \neq 0 \qquad [5]$$

where $\underline{b}$ is the dislocation Burgers vector and $\underline{n}$ is the normal to the reflecting plane (17). Thus, a dislocation does not produce an image when its Burgers vector lies in the reflecting plane. The possible Burgers vectors of dislocations in the basal slip system of a HCP material are the edges of the hexagon shown in Figure 4, and they

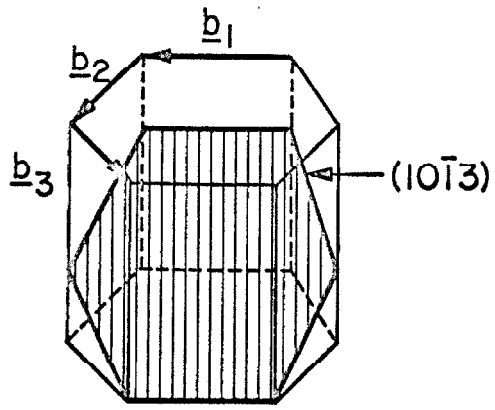

Reflecting Plane No. 1

(a) (10$\bar{1}$3) Reflecting Plane

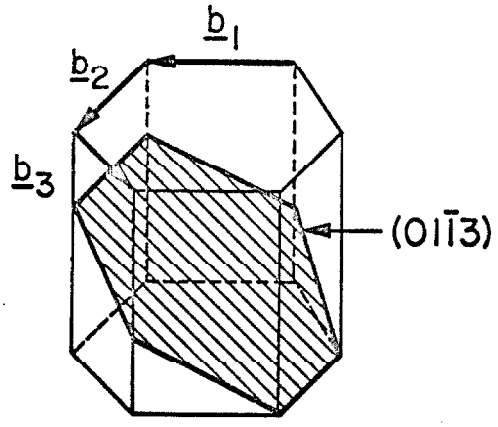

Reflecting Plane No. 2

(b) (01$\bar{1}$3) Reflecting Plane

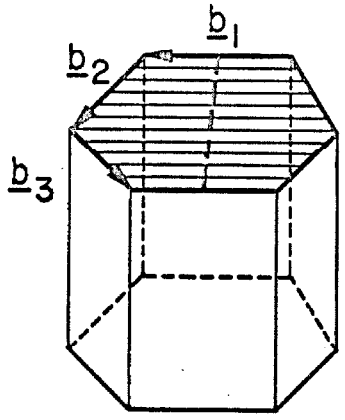

(c) Scratch along [10$\bar{1}$0] on a Basal Plane

Figure 4. Schematic Diagram Showing Relative Orientation of Dislocation Burgers Vectors, Reflecting Planes, and Scratch on Basal Plane.

may be designated as $\pm\underline{b}_1$, $\pm\underline{b}_2$, and $\pm\underline{b}_3$. X-rays from reflecting plane no. 1, the $(10\bar{1}3)$ plane, do not reveal dislocations having Burgers vectors $\pm\underline{b}_1$ because $\pm\underline{b}_1$ lie in the reflecting plane. However, dislocations with Burgers vectors $\pm\underline{b}_2$ and $\pm\underline{b}_3$ are revealed because these Burgers vectors satisfy equation 4. Likewise, if reflecting plane no. 2 is used, dislocations with Burgers vectors $\pm\underline{b}_2$ are not revealed, but those with Burgers vectors $\pm\underline{b}_1$ and $\pm\underline{b}_3$ are revealed. For example, if a given basal dislocation is revealed when reflecting plane no. 1 is used but it is not revealed when no. 2 is used, then the dislocation Burgers vector must be $\pm\underline{b}_2$. There is no way to tell the sign of $\underline{b}$ from Berg-Barrett photographs. Figure 5 shows two enlargements (75X) of Berg-Barrett photographs of the same scratch on the basal plane of a zinc specimen. The scratching and photographing were done as described earlier in this thesis. The photograph on the left in Figure 5 was taken by using the $(01\bar{1}3)$ reflecting planes while the one on the right was taken by using the $(10\bar{1}3)$ reflecting planes. The scratch was made parallel to the $[10\bar{1}0]$ direction, as shown in Figure 4c. Since the dislocations around the scratch are revealed in the $(01\bar{1}3)$ reflection but not in the $(10\bar{1}3)$ reflection, the dislocations have the Burgers vector $\pm\underline{b}_2$, i.e., $\pm 1/3\ [\bar{1}\bar{2}10]$. Also, since the Burgers vector of these dislocations is normal to the dislocation lines, the dislocations are of edge orientation. Scratches with this orientation were used in all the work reported in this thesis.

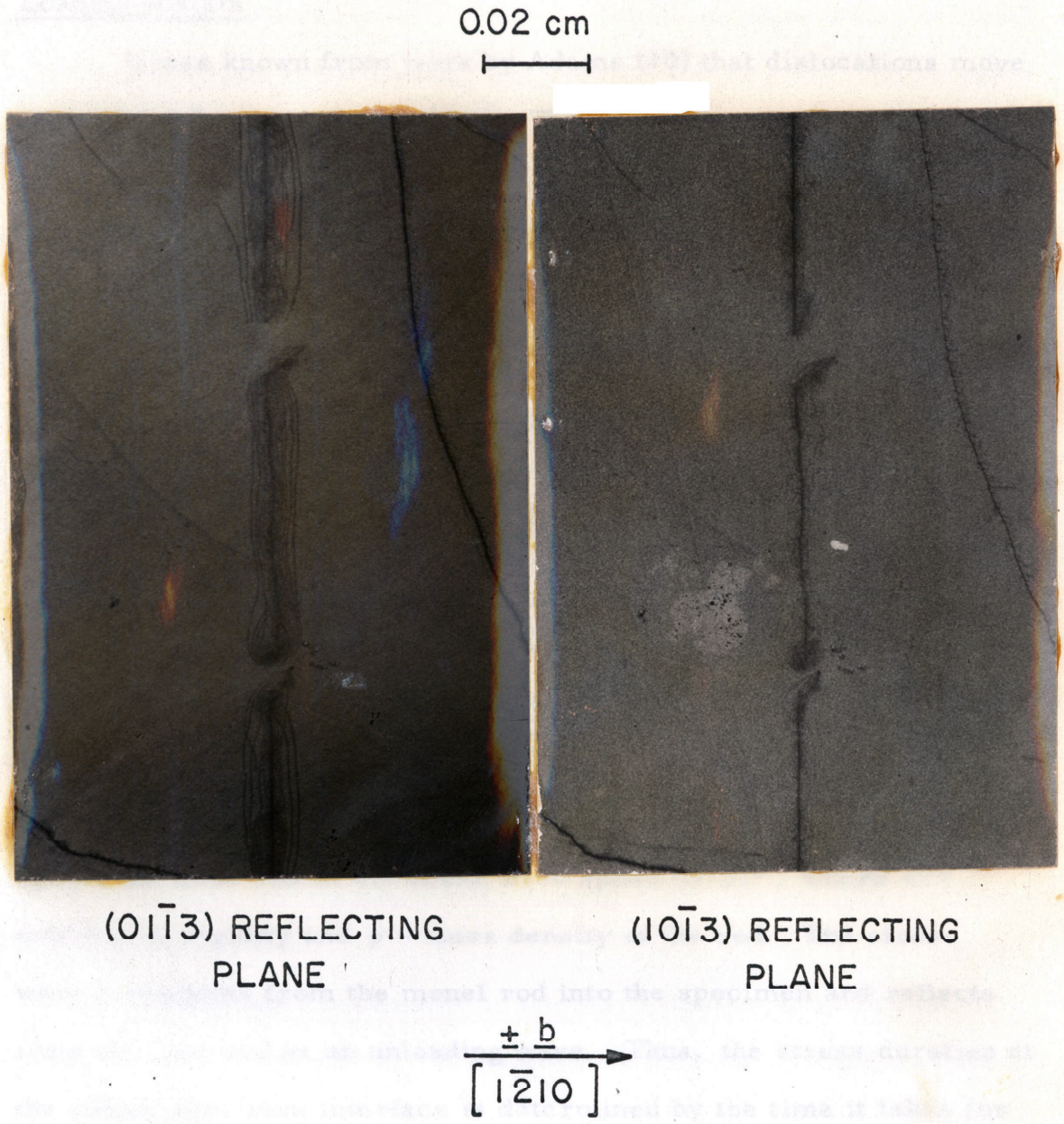

Figure 5. Two Berg-Barrett Photographs of the Same Area Using Two Different Reflecting Planes. Scratch Is Along [10$\bar{1}$0].

Loading System

It was known from work by Adams (10) that dislocations move very fast at low stresses in zinc. Therefore, it was necessary to devise a loading system to apply one stress pulse of microsecond duration to the specimens, so that the dislocations being observed would not move out of the specimens during loading. Loading times of such short duration can be obtained only by stress wave propagation techniques. A machine was constructed by Pope, Vreeland, and Wood (18) which utilizes non-dispersive zero mode torsional waves in cylindrical rods.

The specimens were loaded in the following manner. The specimen is glued to a polycrystalline monel R405 rod which is part of the loading machine. The c axis (hexagonal axis) of the specimen is parallel to the rod axis. A step input of torsional stress is applied to the monel rod by the torsion loading machine and this stress propagates down the rod at the shear wave speed $(G/\rho)^{\frac{1}{2}}$, where G = modulus of rigidity and ρ = mass density of the rod. The stress wave propagates from the monel rod into the specimen and reflects from the free end as an unloading wave. Thus, the stress duration at the monel-specimen interface is determined by the time it takes for the elastic shear wave to propagate to the specimen free end and return if the plastic strain in the specimen is small. The symmetry of the elastic properties of hexagonal crystals, such as zinc, is such that torsion about the hexagonal axis produces the same elastic stress distribution as that in an elastically isotropic material. Thus, the spatial distribution of stress associated with the elastic wave in the

specimen consists of a shear stress on the basal plane which is linearly proportional to the radius, as given by equation 4. The stress was measured by using 500-ohm semiconductor strain gages with a 0.125 cm gage section glued to the monel rod 0.150 cm from the monel-specimen interface. The gage output was monitored on an oscilloscope as described in reference 18.

The stress duration determined by the round-trip travel time of a torsional wave through the length of a specimen was not long enough to allow dislocation displacements of the desired magnitude. Longer specimens could have been prepared, but it was easier to increase the effective specimen lengths by glueing titanium rods to the specimen free end. Titanium was used for the extenders because its low density results in a low tensile stress in the monel-zinc glue bond. Figure 6 shows a photograph of a monel gage bar - specimen - titanium extender combination. The upper section is the monel gage bar; the short, middle section is the specimen; and the lower bar is the titanium extender.

The change of diameter at the zinc-titanium interface is necessary in order to prevent stress wave reflections at that location. It can be shown that a torsional wave will not be reflected at the interface of two cylindrical bars of different radii if the wavelengths are long compared to the radius change and if the quantity

$$Z = a^4(G\rho)^{\frac{1}{2}} \qquad [6]$$

is continuous across the interface. Z is the torsional acoustic impedance, a is the bar radius, ρ is the mass density, and G is the modulus of rigidity. Thus, a slight change in diameter is made at the

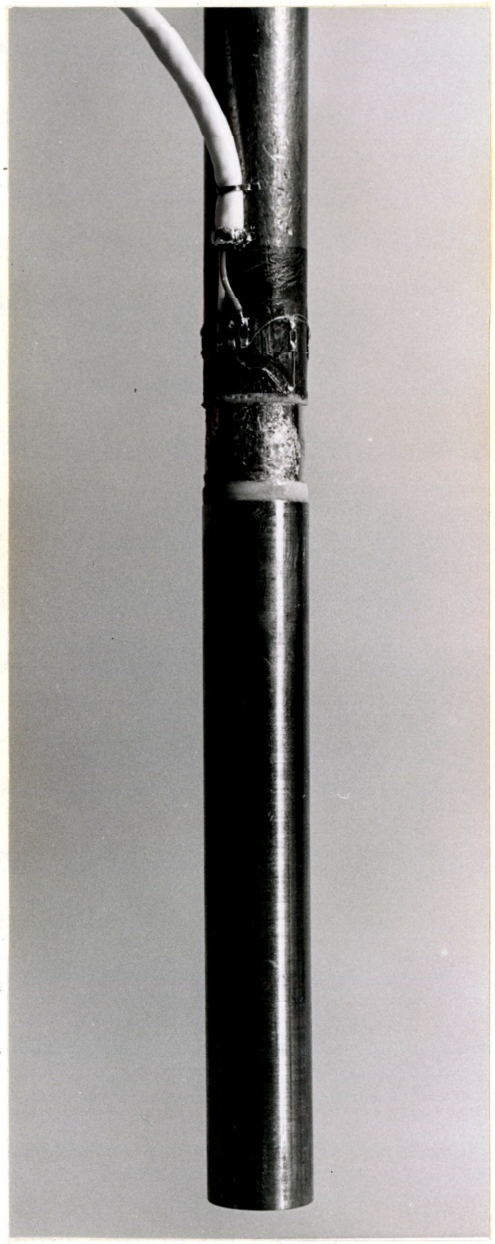

Figure 6. Test Specimen Glued Between Monel Strain Gage Rod and Titanium Extender.

zinc-titanium interface to make Z continuous. However, it was not desirable to have a change in diameter at the monel-zinc interface since it was important to avoid local perturbations in the stress state at this location. Consequently, the radii of the monel and zinc were made the same, resulting in a partial reflection of the wave front at this interface. However, this reflection caused no difficulty since the calibrated strain gages at the interface recorded the actual stress at the specimen surface.

Gluing Technique for Fastening Specimens to Torsion Machine

Since the dislocation displacements were measured on the face of the specimen glued to the torsion machine, it was imperative that plastic strains were not introduced to that face by the gluing process or by differential thermal expansion. Thermal strains were avoided by gluing the observation surface of the specimen to monel R405, an alloy whose coefficient of thermal expansion closely matches that of zinc in the basal plane. The gluing problem, probably the most difficult experimental problem of this work, took considerably more effort to solve.

The glue had to satisfy the following requirements.

1. The glue bond should be capable of withstanding a shear stress of the order of 10×10^6 dyne/cm^2.

2. The specimen face which was glued to the torsion machine was also the surface through which Berg-Barrett x-ray photographs were taken. Therefore, the glue should be easily removable.

3. Basal dislocations move in zinc at shear stresses as small

as 0.3×10^6 dynes/cm^2. Any shear stress on the basal plane in excess of this amount induced by the gluing or ungluing operations would cause uncontrolled dislocation motion. Therefore, stresses due to volume changes in the glue should be very carefully controlled.

4. The glue bond should be void-free to prevent stress concentrations.

The common glues that were tried were found to be unusable because they either changed volume as they set causing large stresses in the specimen, or caused voids in the bond, or produced bonds which were not easily broken. After much experimentation it was found that phenyl salicilate (salol), an organic crystalline material, is a very satisfactory glue, even though it undergoes a large volume change upon solidification; however, it must be used in the following way. The specimen surface to be glued to the loading fixture is first covered with a void-free layer of salol crystals 0.01 cm ± 0.0015 cm thick by spraying the specimen with a solution of 2 gm of salol in 25 ml of acetone with an artist's air brush. The surface of the monel to be glued to the salol is separately coated with molten salol at a temperature slightly above its melting point (46°C). The monel and salol are then cooled to room temperature. The salol coating remains in the liquid state (supercooled) until it is brought into contact with the solid salol-covered zinc surface. The two surfaces are brought into contact with a relative velocity of about 10 cm/min. The layer of solid salol serves to nucleate the solidification of the liquid salol simultaneously over the entire surface to be bonded. The bond is formed very rapidly with a thickness of about 0.025 cm. The thick-

ness of the layer of solid salol is fairly critical, since a layer thicker than 0.01 cm results in a weak glue bond while a thinner layer results in damage to the specimen. The salol glue bond is readily dissolved by soaking the assembly for about 5 minutes in acetone. Berg-Barrett photographs of dislocations around fresh scratches showed only minor changes in dislocation positions due to the above gluing and ungluing operation. These changes were less than 0.002 cm.

Experimental Procedure

Berg-Barrett x-ray photographs were taken of annealed and scratched specimens prior to testing to determine the initial dislocation configuration around the scratches. However, the time required to take the photographs was sufficient for the dislocations around the scratches to become relatively immobile, presumably due to pinning by point defects. Consequently, specimens were stressed in the torsion loading machine immediately after scratching without taking an initial Berg-Barrett photograph. The time between scratching and loading was typically about an hour. Berg-Barrett photographs were taken of the specimens immediately after loading to determine the final dislocation configuration around the scratches. The method used for separating the dislocation displacements due to the scratching operation from the displacements due to the stress pulse is described in the next part of this thesis.

Three specimens were tested, one having an acid-lapped observation surface and two having cleaved observation surfaces. The

shear stress on the periphery of the specimens ranged from 9.7 to 17.2×10^6 dynes/cm^2. The combined length of the specimens and titanium rods were such that the load duration at the observation surface (interface between the specimen and the monel bar) ranged from 47 to 94 μsec. The output of the strain gages on the monel bar was monitored on an oscilliscope during each test.

IV. EXPERIMENTAL RESULTS

Dislocation Displacement Measurements

Figure 7a shows the dislocation configuration around a scratch on an untested specimen. A Berg-Barrett photograph of the dislocation configuration around three scratch segments on a tested specimen is shown in Figure 7b. The maximum distance of dislocations from each scratch segment was measured on the Berg-Barrett photographs by means of a filar eyepiece on a microscope. The measurements were made at every scratch segment at which the displacements were measureable. Measurements were not made on scratch segments where the dislocation motion appeared to be impeded by sub-boundaries. The results of these measurements are shown in Figure 8 plotted as a function of radial position on the specimen. Each plotted point represents a measurement of a maximum dislocation distance from a scratch segment after loading. Within experimental scatter, the distance of the dislocation farthest from the scratch after stress application is linearly proportional to radial position, as indicated by the line drawn in each plot.

The measured maximum displacement, D_m, of a dislocation from a scratch segment after testing is the sum of two displacements,

$$D_m = D_o + D \qquad [7]$$

where D_o is the displacement from the scratch produced by the scratching operation and D is the displacement produced by the torsional loading. Since Berg-Barrett photographs were not taken of the scratched specimens prior to leading, D_o could not be measured

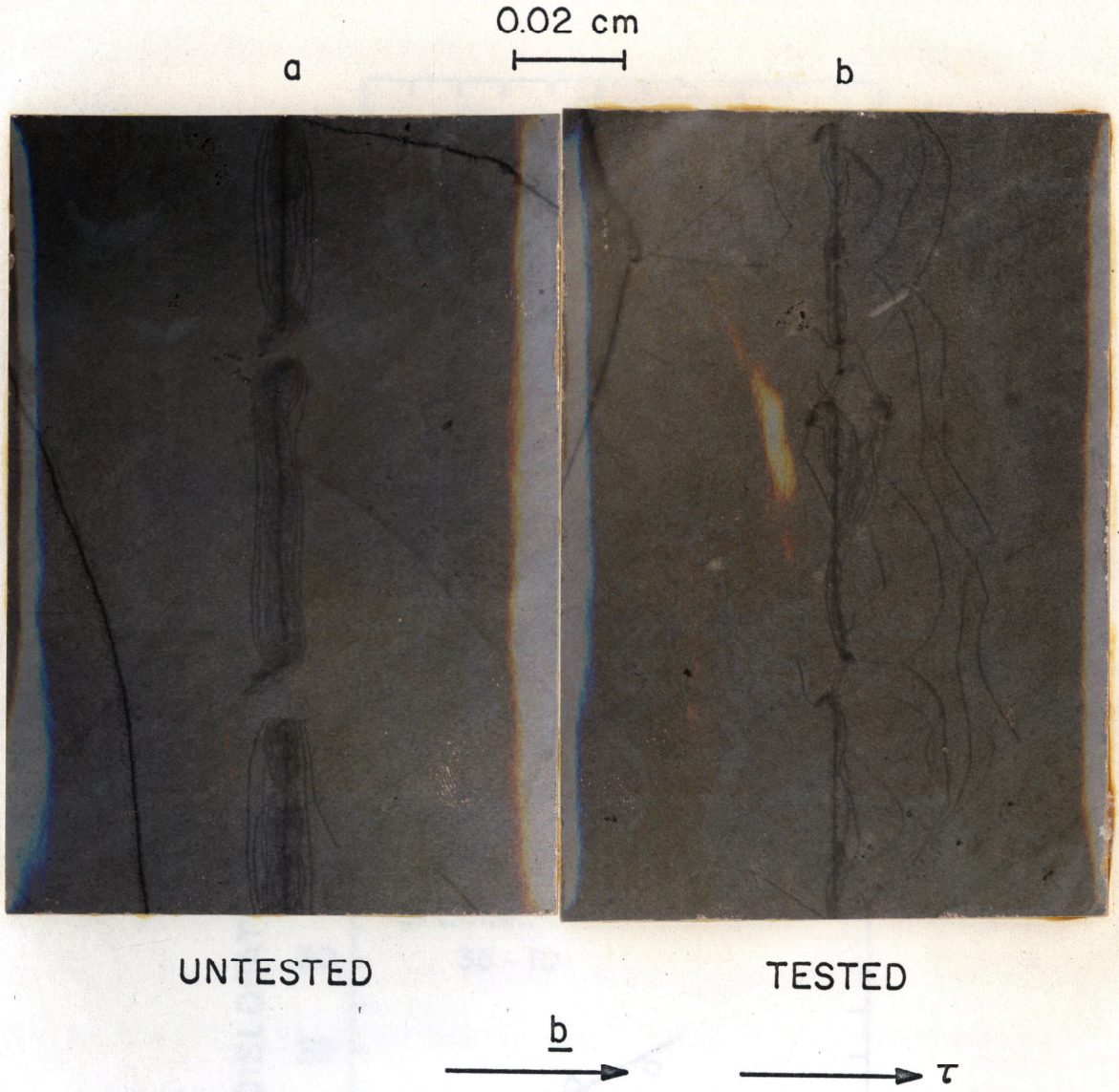

Figure 7. Berg-Barrett Photographs of Dislocations Around Scratch Segments on a Tested and an Untested Specimen. (Two Different Specimens.)

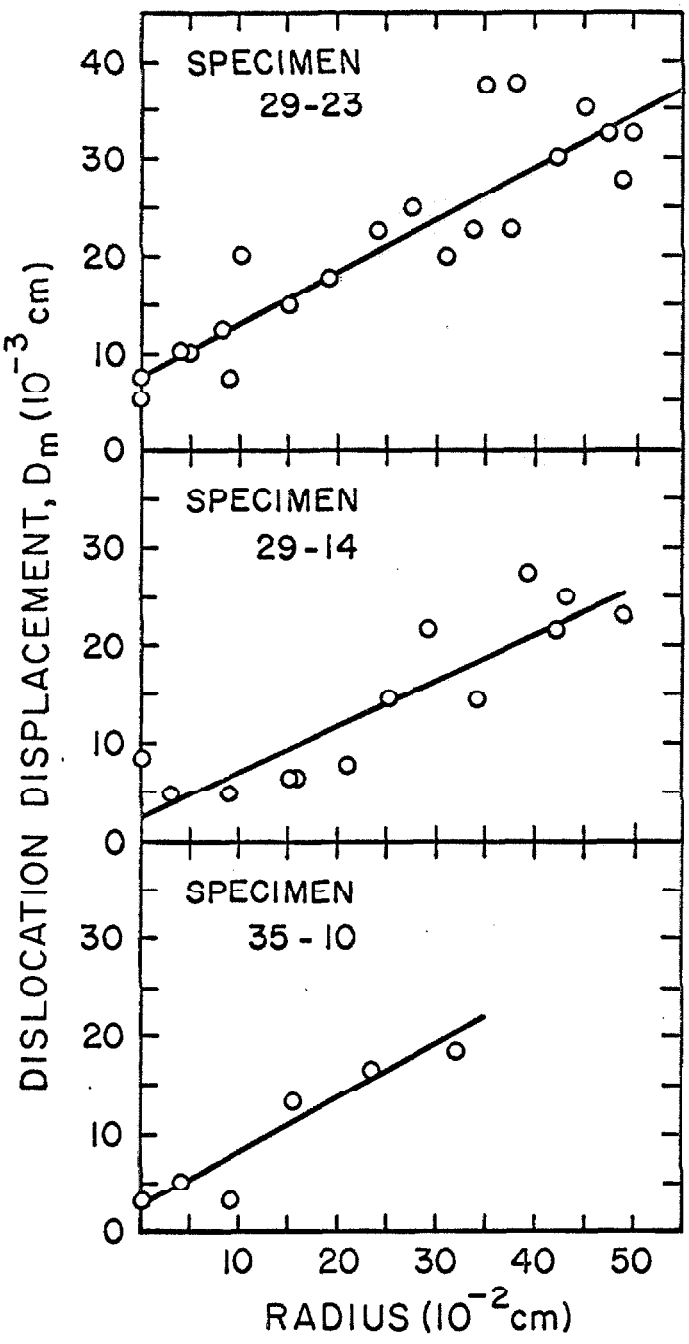

Figure 8. Dislocation Displacement Plotted Against Radial Position on Specimen where Displacement Was Measured.

directly. Therefore, it was necessary to determine D_o indirectly. The value of D_o used in these measurements is the value of D_m at $r = 0$ for each of the plots in Figure 8. The value of D_m at $r = 0$ should be D_o, since the applied shear stress is zero at $r = 0$. The values of D_o determined in this manner do not allow for a variation of D_o for different scratch segments, but they are compatible with measurements made on Figure 7a. In Figure 7a the maximum distance of dislocations from the scratch furrows is $5 \times 10^{-3} \pm 2.5 \times 10^{-3}$ cm.

Since all radial positions on each specimen experienced the same load duration, the dislocation velocity is given by D/(load duration). If the plastic strains are small the applied shear stress is a linear function of radial position as given by equation 4. Since D is a linear function of radial position, as shown in Figure 8, then dislocation velocity is a linear function of applied shear stress.

It should be noted that the dislocations shown in Figure 7b moved in the direction of the applied resolved shear stress as would be expected from the following argument. The Al_2O_3 whisker produces a furrow in the specimen similar to the one shown schematically in Figure 9 on a greatly expanded scale. The most plausible means for accommodating at least some of this deformation is by the production of edge dislocations of the same sign on either side of the furrow as shown. Since the dislocations on opposite sides of the scratch are of the same sign, they should move in the same direction when the shear stress is applied. Furthermore, dislocations of this sign should move in the direction of the applied shear stress, as the

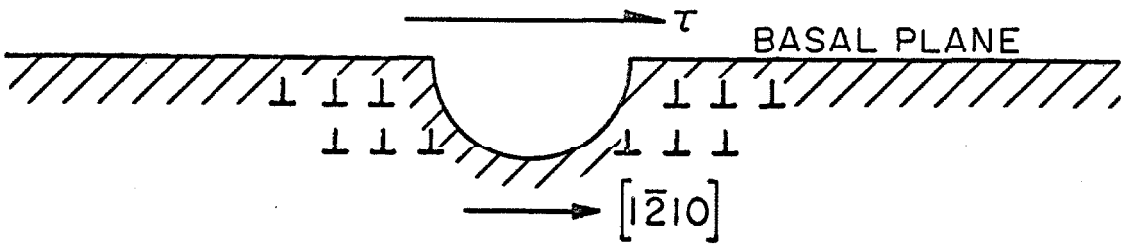

Figure 9. A Possible Dislocation Configuration Around a Furrow Caused by Scratching a Basal Plane Along [10$\bar{1}$0].

dislocations do in Figure 7b. There were isolated instances of motion in the opposite direction, indicating the generation of some dislocations of opposite sign. However, almost all of the displacements were in the direction shown in Figure 7b. The dislocation motions should also have the same cylindrical symmetry that the applied shear stress has in torsion, i.e., the dislocations on opposite sides of the specimen center should move in opposite directions. This is observed.

Stress and Time Measurements

The stress pulse magnitude and duration must be known in order to determine dislocation velocity as a function of applied shear stress from the dislocation displacement measurements. Figure 10 shows four records of the strain gage output for four different stress pulses. The top trace in each photograph shows the strain-time history in the monel bar over a period of 2 millisec while the bottom trace shows the main pulse in the top trace on an expanded time scale. The top traces show that only one pulse of significant amplitude is applied to the specimen. The record in Figure 10a shows the shape of a pulse which occurs when a titanium extender is glued directly to the monel strain gage bar without a specimen in between. The salol glue layer was made very thin to minimize effects of the large compliance of the salol. The titanium extender was made 1.15 cm in diameter so that its torsional acoustic impedance is the same as the 1.10 cm diameter zinc specimens. Therefore, the strain gage output in Figure 10a is the same as for a zinc specimen behaving

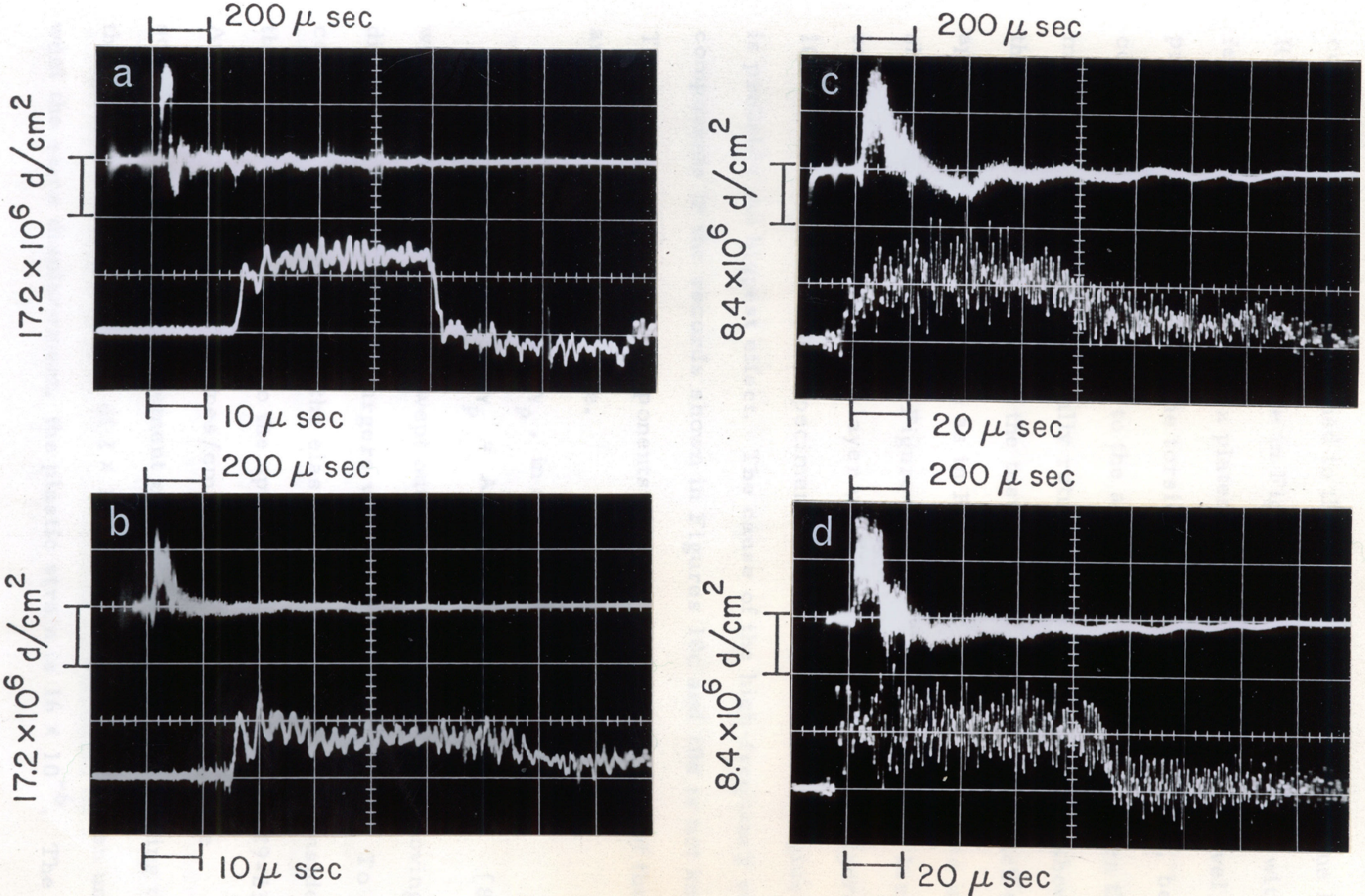

Figure 10. Four Strain Gage Records; (a) = record obtained with titanium extender glued directly to monel strain gage bar; (b), (c), (d) = records from tests on specimens 29-23, 29-14, and 35-10, respectively.

completely elastically fastened to the monel rod with a thin glue layer. Referring to the bottom trace in Figure 10a, the stress rises within a few microseconds, reaches a plateau with some changes in level probably due to friction in the torsion machine, drops to zero, becomes slightly negative due to the acoustical mismatch between the monel and titanium, and finally returns to zero. Figure 10b shows the strain gage record from the test on specimen 29-23 in which the applied torque was the same as in Figure 10a. The differences in shape between the pulses in Figure 10a and 10b are due to the large compliance of the thick glue layer used in the test shown in Figure 10b and plastic flow in the specimen. The compliance of the glue bond is probably the biggest effect. The cause of the high-frequency stress components in the records shown in Figures 10c and 10d is not known. The amplitude of these components seems to be independent of the amplitude of the input torque.

The plastic strain, γ_p, in a specimen is given by

$$\gamma_p = Ab \quad , \qquad [8]$$

where A is the total area swept out per unit volume by the moving dislocations and b is the Burgers vector of the dislocations. To compare the magnitudes of the elastic and plastic strains, consider the dislocation motion due to the applied stress on specimen 29-23. At a stress of 11.3×10^6 dynes/cm^2 the dislocations from the scratch underwent a displacement of about 0.030 cm. Assuming that the entire dislocation length of 2×10^4 cm/cm^3 in the specimen underwent the same displacement, the plastic strain is 16×10^{-6}. The

elastic strain corresponding to a shear stress of 11.3×10^6 dynes/cm^2 is 29×10^{-6}. The plastic strain must be far smaller than 16×10^{-6} since the dislocations in the bulk of the crystal are not all mobile nor are they all oriented such as to be moved by the maximum shear stress. Therefore, the plastic strain is considerably smaller than the elastic strain, so the assumption that the spatial stress distribution in the specimen is the elastic stress distribution is probably a good one.

The results presented in Figure 10 indicate that the dislocation velocity is a linear function of applied stress. Therefore, the dislocation displacements at any radial position are directly proportional to the time integral of the stress at that radius, where the integral is taken over the total duration t_1 of the stress pulse, i.e.,

$$D = \int_0^{t_1} v(t)dt = K \int_0^{t_1} \tau(t)dt = K\tau_{eff}t_o \qquad [9]$$

where $v(t)$ = instantaneous dislocation velocity,

K = constant

$\tau(t)$ = instantaneous stress,

τ_{eff} = effective stress for a square pulse of duration t_o,

and t_o = round trip travel time of an elastic wave through the specimen and titanium extender.

The effective stress at the maximum radius was determined for each specimen by performing the time integral of stress on each stress record with a planimeter and dividing the integral by t_o. Values of τ_{eff} and t_o are given in Table I.

TABLE I

Specimen	τ_{eff} (10^6 dynes/cm^2) maximum	t_o (μ sec)
29-23	17.3	47
29-14	12.8	73
35-10	9.7	94

Dislocation Velocities

Dislocation velocities were calculated by dividing D, the dislocation displacement due to the load pulse, by the pulse duration t_o. The dislocation velocity-stress data are plotted in Figure 11. The velocities were determined as described above and the associated stresses are the effective stresses also determined as described above, assuming that the shear stress is a linear function of radius. Velocities were calculated only for those values of $D \geq 2 \times 10^{-3}$ cm since the uncertainty in D_o makes the relative error in D unreasonably large for $D < 2 \times 10^{-3}$ cm. The data in Figure 11 are fitted with the straight line

$$v = 3.4 \times 10^{-5} \tau \qquad [10]$$

where v is in cm/sec and τ is in dynes/cm^2. The line was determined by making the algebraic sum of the deviations of the data from the line equal to zero. Other straight lines with different slopes and intercepts or higher degree curves might be used to fit the data, but the scatter of the data does not seem to warrant a more precise fit.

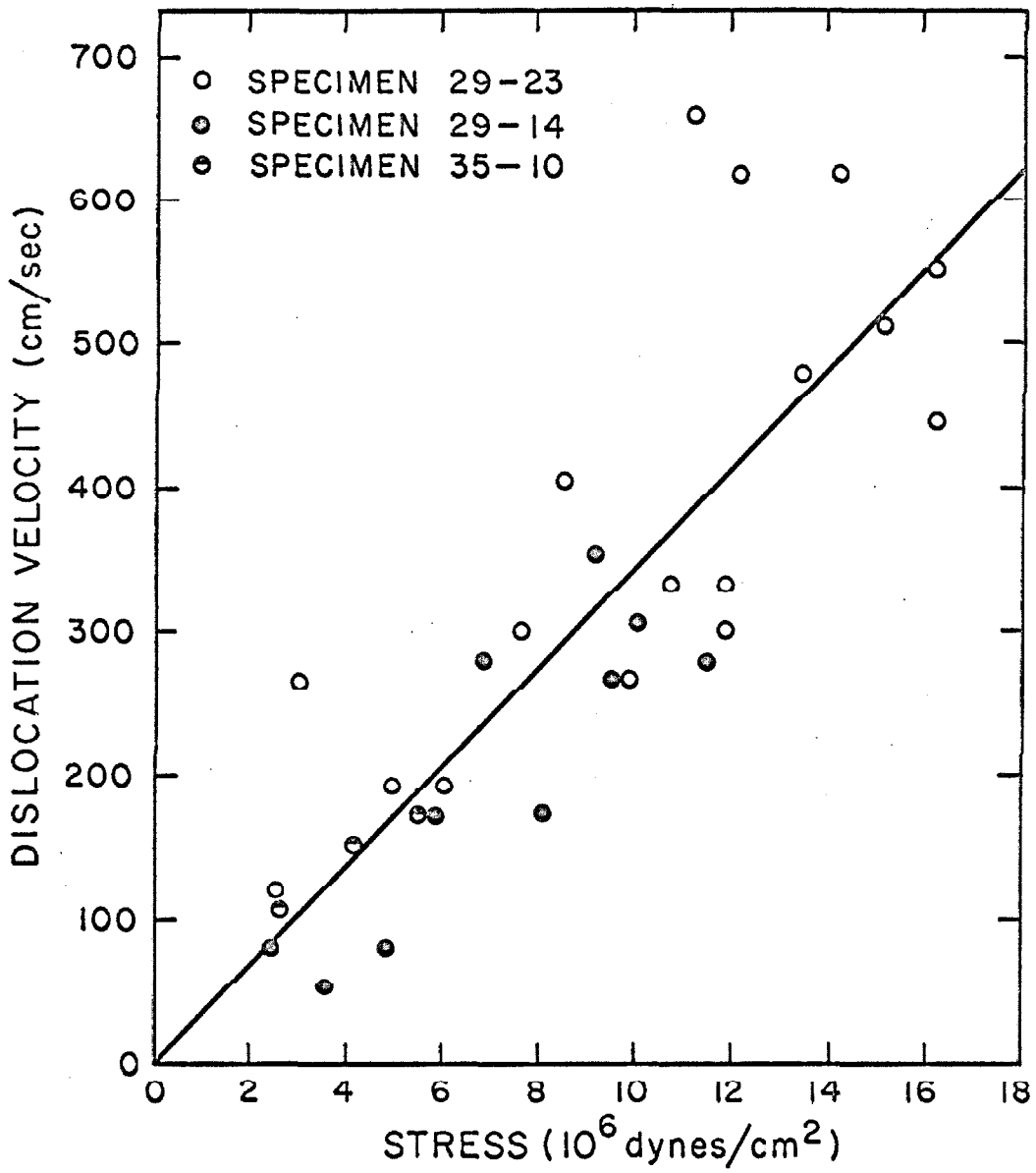

Figure 11. Plot of Measured Dislocation Velocity as a Function of Applied Resolved Shear Stress.

V. DISCUSSION

Effect of Line Tension

The line tension of a curved dislocation could influence the results of this study by modifying the net force on the dislocation. The magnitude of this effect is estimated here. The energy per unit length of a dislocation is conveniently represented in terms of a line tension. This line tension exerts a force on a curved segment of a dislocation line in addition to those forces which the applied shear stress exerts. The stress required to maintain a segment of dislocation with a radius of curvature r in equilibrium is approximately given by

$$\tau = \frac{Gb}{2r} \qquad [11]$$

where G is the modulus of rigidity and b is the dislocation Burgers vector.

A typical radius of curvature of the dislocations on a tested specimen is 0.018 cm as determined from Figure 7b. The stress required to maintain this radius is about 0.3×10^6 dynes/cm^2, a small stress compared to the applied stresses in this work. The radii of curvature of dislocations around a scratch on an untested specimen are larger than 0.018 cm except near the ends of the scratch segments, as can be seen in Figure 7a. Therefore, the effect of dislocation line tension is negligible compared to that of the applied stresses in this work.

Effect of Dislocation Interactions

The stress fields of nearby dislocations can materially affect the stress acting on a dislocation. The magnitude of this effect is

calculated and compared to the applied shear stress to determine how this effect might influence the data. The dislocations around the scratch on an untested specimen, shown in Figure 7a, are spaced about 6×10^{-4} cm apart. If all these dislocations are of the same sign and lie on the same slip plane, the dislocation farthest from the scratch experiences a shear stress of about 7×10^{6} dynes/cm^2, tending to move it away from the scratch. Adams (10) observed large dislocation displacements at stresses as low as 0.5×10^{6} dynes/cm^2 and motions were observed in the present investigation at stresses as low as 1.3×10^{6} dynes/cm^2. The fact that dislocations move at stresses considerably less than 7×10^{6} dynes/cm^2 indicates that the dislocations around the scratch on an untested specimen must not be coplanar or the outermost dislocation would move considerably farther from the scratch. The dislocation spacing in Figure 7a is about the same magnitude as the x-ray penetration depth. Therefore, the dislocations seen around the scratch are probably on different planes which are from 0 to 5 μ below the free surface. If the dislocations are on different slip planes the stress on the dislocation farthest from the scratch is considerably reduced from 7×10^{6} dynes/cm^2. Most of the dislocation displacements measured were large compared to 3×10^{-4} cm and therefore dislocation interactions had an effect over only a small portion of the motion. Therefore, dislocation interaction effects are believed to be small.

Effect of Pinning Due to Point Defects

The dislocation velocity at a given applied shear stress may

be influenced by the presence of point defects in the dislocation core. The pinning of dislocations that occurs when specimens are aged before testing is probably due to the diffusion of point defects to the dislocations from the specimen surface. The effect of drag due to these defects on the data presented in this thesis cannot be assessed. Every attempt was made to minimize the aging time before testing to minimize the number of these defects.

Comparison of This Work with Previous Work

Adams (10) measured the rate of growth of slip bands in zinc. He employed compression stress pulses and used an etch to reveal the dislocations in the slip bands formed by the stress pulses. The dislocation velocities observed by Adams agree in magnitude with the velocities observed in the present work at comparable stress levels. However, scatter and the relatively small velocity range covered in Adams' data makes comparison difficult. The scatter and restricted range of measurements in Adams' data are also believed to be the reason why his mobility function differs from the one presented in this thesis. The loading machine used by Adams produced load pulses with a minimum duration of 17 millisec, long enough for many of the slip bands he observed to move completely across his specimens. This placed a limitation on the maximum velocity that he could observe and indicated the need for the torsion loading system developed in this investigation.

Mechanisms for Limiting Dislocation Velocities

A number of theories predict dislocation mobility by assuming

that the dislocations move in jumps from one obstacle to the next, and that the combined effect of thermal activation and the applied shear stress are required for the dislocation to overcome the obstacle. Various kinds of obstacles have been treated including point defects (19, 20) and forest dislocations (21).

The analysis of Gilman (19),who treated the release of dislocations from point defect pinning, predicts dislocation velocity to be given by

$$v = c_s e^{-D/\tau} \qquad [12]$$

where τ is the applied, resolved shear stress, c_s is the shear wave speed of the material, and D is a constant. However, the data obtained in the present work do not fit the functional form of equation 12. Also, an extrapolation of the curve for large τ on this plot yields $v \approx 3 \times 10^3$ cm/sec, which is far below $c_s = 2.3 \times 10^5$ cm/sec predicted by equation 12.

The theory of Fleischer (20) is based on the interaction of dislocations with point defects which produce large tetragonal lattice strains. These strains are produced, for example, in LiF by a Ca^{++} ion and an associated vacancy. Such defects are not thought to exist in 99.999 per cent purity zinc.

The theory of Seeger, et al. (21) is based on the interaction of basal dislocations with non-basal (forest) dislocations. This theory predicts that basal dislocation velocities are given by

$$v = D e^{\tau/kT} \qquad [13]$$

where τ is the applied shear stress, D is a constant, and k is

Boltzmann's constant. The data obtained in the present investigation do not fit such a functional form.

Another group of theories considers dislocation velocities to be limited by the interaction of the moving dislocation strain field with vibrations of the crystal lattice. The theory has been approached in various ways by Leibfried (22), Eshelby (23), Mason (24), and has recently been unified and extended by Lothe (25). Four different sources of dislocation drag have been treated; the thermoelastic effect, the core anharmonicity effect, the phonon viscosity effect, and the phonon scattering effect. According to Lothe, the thermoelastic effect is negligible in metals while the other three effects give rise to drag stresses of approximately the same magnitude. The total drag stress τ_D on a moving dislocation due to these three effects is

$$\tau_D \approx \frac{3}{10} \frac{\epsilon v}{c_s} \quad . \qquad [14]$$

ϵ is the thermal energy density, $\frac{3kT}{V}$; k is Boltzmann's constant; V is the volume per atom = 14.7×10^{-24} cm^3 in zinc. c_s is the shear wave speed = 2.3×10^5 cm/sec. This theory is attractive because it not only predicts the observed linear dislocation velocity-stress function but also predicts the correct order of magnitude of the constant of proportionality. Equation 14 predicts

$$v \approx 9 \times 10^{-5} \tau \quad . \qquad [15]$$

at room temperature with c_s taken as 2.3×10^5 cm/sec. This is to be compared to equation 10,

$$v = 3.4 \times 10^{-5} \tau \quad . \qquad [10]$$

the experimentally determined relation. Considering that equation 14

yields only an order of magnitude estimate of the proportionality constant, the agreement between this theory and the present experimental results is very good.

Those theories which depend upon thermal activation for dislocations to overcome obstacles predict that dislocation velocities increase with increasing temperature. However, the phonon drag theory predicts that dislocation velocities decrease with increasing temperature. The results of tests at different temperatures would help greatly in establishing the correct mechanism.

Comparison of Dislocation Mobilities in Zinc with Mobilities in Other Materials

As stated earlier in this thesis, dislocations in copper and zinc move considerably faster than 1 cm/sec at the macroscopic yield point. In all other materials on which mobility data have been gathered, dislocations move considerably slower than 1 cm/sec at the macroscopic yield point. This distinction is more clearly indicated in Table II, wherein the results of most of the mobility measurements made to date are summarized. The mobility exponent m in the table is the exponent in equation 3.

Greenman (11) found that the dislocations in copper obey the relation

$$v = 3.6 \times 10^{-5} \tau \quad . \qquad [16]$$

The similarity of dislocation mobilities in zinc and copper as seen by comparison of equations 10 and 16 is striking. The phonon drag theory predicts the mobility of dislocations in copper to be

TABLE II

DISLOCATION VELOCITY AT THE YIELD STRESS

(at room temperature unless otherwise noted)

Material	Yield Stress 10^6 dyne/cm^2	Velocity at Yield Stress cm/sec	Mobility Exponent m	Reference
Tungsten	730	0.001	4.8	7
Lithium Fluoride	88	0.015 (edge) 0.0009 (screw)	25	1
Sodium Chloride (High Purity)	17 2.9	0.00001	8 17	6
Iron - 3% Silicon	1,200	0.0000015	35	5
Germanium (500°C)	280	0.0006	1.9	8
Copper	5	200	1.0	11
Zinc	0.4	15	1	this investigation

$$v = 10^{-4} \tau \ . \qquad [17]$$

Hence, the phonon drag theory predicts velocities that are approximately a factor of 3 too high for both copper and zinc.

Suzuki, et al. (26) have indirectly measured the damping stress on moving dislocations in copper by internal friction techniques. These investigators found that the damping stress on dislocations in copper does increase with increasing temperature, although not in the exact manner predicted by equation 14. It would be very useful and interesting to compare the results of the present investigation with results from internal friction measurements. However, adequate results from internal friction measurements on zinc are not presently available.

VI. SUMMARY AND CONCLUSIONS

Basal dislocations of predominantly edge character were produced within a depth of about 5 μ below the basal plane observation surface of 99.999 per cent pure zinc crystals by controlled scratching of the surface. Movement of these dislocations on their glide planes was produced by resolved shear stresses ranging from 2 to 17×10^6 dynes/cm^2 applied to the crystal surface for load durations ranging from 47 to 94 μsec. The distance through which the dislocations moved was determined from Berg-Barrett x-ray micrographs.

The dislocation velocities determined from the dislocation movement and the duration of stress ranged from 40 to 700 cm/sec and were linearly proportional to the stress. This functional relationship between applied stress and dislocation velocity in zinc was not known prior to this investigation. The experimental value of the ratio of applied resolved shear stress to dislocation velocity, 3.4×10^5 dyne sec/cm^3, is in agreement, within experimental and theoretical uncertainties, with the theoretical value of 9×10^5 dyne sec/cm^3 derived from the concept of the interaction between dislocations and the thermal vibrations of the crystal lattice (phonon drag effect).

Suggested Further Work

There are several experiments that should be performed to extend and refine the data presented in this thesis. Experiments should be performed wherein the mobility of basal dislocations in zinc is measured as a function of temperature to determine the applicability of the phonon drag theory. The mobility of basal dislocations in zinc should also be measured as a function of non-basal

dislocation density and as a function of impurity content. The mobility of screw oriented dislocations should be measured. The dislocation lines at the ends of the scratch segments are screw oriented and the motion of these dislocations can be observed by making the gaps between the scratch segments larger. All these experiments could probably be carried out using essentially the same techniques presented in this thesis.

The results presented in this thesis could be refined in several respects:

(1) A search should be made for a fast film of sufficient resolution so that Berg-Barrett photographs of the scratched specimens could be taken before loading. This would remove the uncertainty concerning the position of the dislocations prior to loading.

(2) A glue of lower compliance than salol should be sought for fastening the specimen to the torsion machine so that the degradation of the stress pulse by the glue joint could be decreased.

(3) Crystals should be produced having lower bulk dislocation content so that the plastic strain that occurs during loading would be smaller. This would make it possible to make mobility measurements at higher applied shear stresses.

LIST OF REFERENCES

1. W. G. Johnston and J. J. Gilman, "Dislocation Velocities, Dislocation Densities, and Plastic Flow in Lithium Fluoride Crystals," J. Appl. Phys. 30, 129 (1959).

2. W. G. Johnston, "Yield Points and Delay Times in Single Crystals," J. Appl. Phys. 33, 2716 (1962).

3. J. C. M. Li, "A Dislocation Mechanism of Transient Creep," Acta Met. 11, 1269 (1963).

4. J. W. Taylor, "Dislocation Dynamics and Dynamic Yielding," J. Appl. Phys. 36, 3146 (1965).

5. D. F. Stein and J. R. Low, Jr., "Mobility of Edge Dislocations in Silicon-Iron Crystals," J. Appl. Phys. 31, 362 (1960).

6. E. Yu. Gutmanas, E. M. Nadgornyi, and A. V. Stepanov, "Dislocation Movement in Sodium Chloride Crystals," Soviet Phys. Solid State 5, 743 (1963).

7. H. W. Schadler, "Mobility of Edge Dislocations on {110} Planes in Tungsten Single Crystals," Acta Met. 12, 861 (1964).

8. A. R. Chaudhuri, J. R. Patel, and L. G. Rubin, "Velocities and Densities of Dislocations in Germanium and Other Semiconductor Crystals," J. Appl. Phys. 33, 2736 (1962).

9. M. N. Kabler, "Dislocation Mobility in Germanium," Phys. Rev. 131, 54 (1963).

10. K. H. Adams, "Dislocation Mobility and Density in Zinc Single Crystals," Ph. D. Thesis, California Institute of Technology, Pasadena, Calif. (1965).

11. W. F. Greenman, "Dislocation Mobility in Pure Copper Single Crystals," Ph. D. Thesis, California Institute of Technology, Pasadena, Calif. (1966).

12. T. Suzuki and H. Kojima, "A New Method and Results of Observation on Dislocation Motion in Silicon Crystals," Technical Report of the Institute for Solid State Physics, Series A, No. 173, the University of Tokyo (1965).

13. R. W. Guard, "Rate Sensitivity and Dislocation Velocity in Silicon Iron," Acta Met. 9, 163 (1961).

14. E. J. Stofel, "Plastic Flow and Fracture of Zinc Single Crystals," Ph. D. Thesis, California Institute of Technology, Pasadena, Calif. (1962).

15. R. C. Brandt, K. H. Adams, and T. Vreeland, Jr., "Dislocations and Etch Figures in High Purity Zinc," J. Appl. Phys. 34, 591 (1963).

16. J. M. Schultz and R. W. Armstrong, "Seeing Dislocations in Zinc," Phil. Mag. 10, 497 (1964).

17. J. B. Newkirk, "The Observation of Dislocations and Other Imperfections by X-Ray Extinction Contrast," AIME Trans. 215, 483 (1959).

18. D. P. Pope, T. Vreeland, Jr., and D. S. Wood, "Machine for Producing Square Torsion Pulses of Microsecond Duration," Rev. Sci. Instr. 35, 1351 (1964).

19. J. J. Gilman, "Dislocation Mobility in Crystals," J. Appl. Phys. 36, 3195 (1965).

20. R. L. Fleischer, "Rapid Solution Hardening, Dislocation Mobility, and the Flow Stress of Crystals," J. Appl. Phys. 33, 3504 (1962).

21. A. Seeger, S. Mader, and H. Kronmüller, "Theory of Work-Hardening of FCC and HCP Single Crystals," Electron Microscopy and Strength of Crystals, Interscience Publ., New York (1963), p. 665.

22. G. Leibfried, "Uber der Einfluss Thermisch angeregter Schallwellen auf der Plastische Deformation," Z. Physik 127, 344 (1950).

23. J. D. Eshelby, "Dislocations as a Cause of Mechanical Damping in Metals," Proc. Roy. Soc. A197, 396 (1949).

24. W. P. Mason, "Phonon Viscosity and Its Effect on Acoustic Wave Attenuation and Dislocation Motion," J. Acoust. Soc. Am. 32, 458 (1960).

25. J. Lothe, "Theory of Dislocation Mobility in Pure Slip," J. Appl. Phys. 33, 2116 (1962).

26. T. Suzuki, A. Ikushima, and M. Aoki, "Acoustic Attenuation Studies of the Frictional Force on a Fast Moving Dislocation," Acta Met. 12, 1231 (1964).